Supplemental Data

Postsynaptic Mad Signaling at the *Drosophila* Neuromuscular Junction

Veronica Dudu, Thomas Bittig, Eugeni Entchev, Anna Kicheva, Frank Jülicher, and Marcos González-Gaitán

Supplemental Experimental Procedures

The "Immobile" Nuclear Mad Pool

The immobile pool in FRAP experiments reveals the existence of double kinetics: fast kinetics that causes recovery within the time scale of the experiment, and slow kinetics that will lead to recovery to the initial values after a much longer time. In order to address whether the immobile pool consists of Mad molecules bound to a static structure inside the nucleus (e.g., DNA), FRAP experiments were performed in which the fluorescence of a small region within the nucleus was bleached and its recovery kinetics were followed for a short period of time (up to 200 s) (Figures S5A and S5B). We reasoned that analyzing the fluorescence recovery of a smaller region with respect to the whole nucleus would allow us to distinguish between the flow of molecules into/out of the nucleus and the movement of the fluorescent molecules within the nucleus. Both the control and Tkv^{QD} recover to the total nuclear concentration (Figure S5D). The fluorescence recovery in the bleached region could be explained either by the movement of the chromatin inside the nucleus together with bound P-Mad* or by the free movement of the P-Mad* inside the nucleus. When we performed the same type of FRAP experiment with a fluorescent fusion of the Histone 2A, we observed that within the bleached region, the fluorescence does not recover (not even after 20 min) (Figures S5C and S5D and not shown). Since Histone 2A is a stable component of the chromatin (reviewed by [S1]), this result is consistent with the idea that the chromatin is stationary in interphase nuclei. Thus, P-Mad* molecules moving freely, but confined within the nucleus, constitute a pool that most likely fills and empties with slow kinetics and which can therefore account for the existence of the "immobile" fraction.

Effective Import and Export Rates

The FRAP experiments can be analyzed by a theoretical description that is based on the assumption of the existence of three different Mad pools: a mobile and an immobile nuclear pool and a cytosolic pool (Figure 5A). The exchange between the mobile nuclear pool (with concentration n_{mob}) and the cytosolic pool (with concentration c) is determined by the effective import (K_{i}) and export (K_{e}) rates, whereas the immobile nuclear concentration (n_{im}) is assumed to be constant during the experiment. Moreover, we assume that the cytosolic concentration does not change during the time course of the FRAP experiment (1000 s), because the volume of the cytosol is 2 to 3 orders of magnitude larger than that of the single bleached nucleus. Indeed, the pool of cytosolic molecules does not change significantly during the recovery process, because the total number of molecules in the cytosol exceeds the number of molecules in the nucleus by a factor of 124 (control) and 26 (Tkv^{QD}), respectively. Hence, the FRAP kinetics is described by:

$$\begin{aligned} \frac{dn_{\mathrm{mob}}}{dt} &= K_{\mathrm{i}}c - K_{\mathrm{e}}n_{\mathrm{mob}} \\ \frac{dc}{dt} &= 0 \\ \frac{dn_{\mathrm{im}}}{dt} &= 0. \end{aligned} \tag{6}$$

The solution to the equation describing the recovery of the mobile pool is

$$n_{\mathrm{mob}}(t) = n^{\mathrm{s}}_{\mathrm{mob}}\left(1 - (1-b)e^{-K_{\mathrm{e}}t}\right), \tag{7}$$

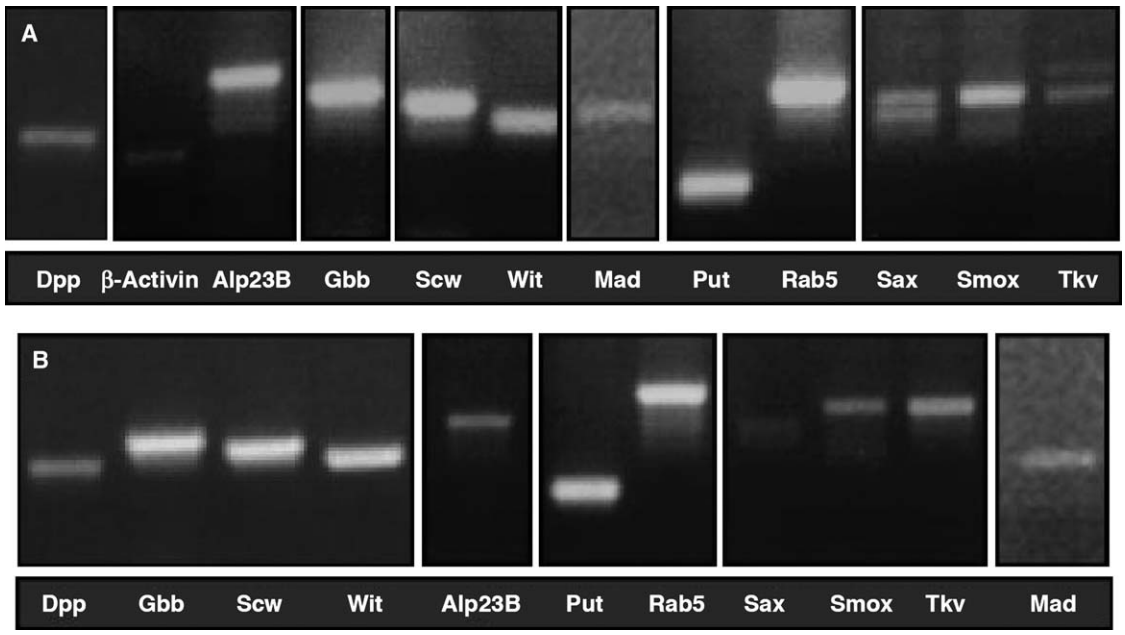

Figure S1. TGF-β Superfamily Ligands, Receptors, and Transcription Factors Are Transcribed in *Drosophila* Brain and Muscles

RT-PCR of 3rd instar larval brains (A) and muscles (B). Note that the muscle preparation corresponds to a fillet, which might include hypodermis and sensory neurons in addition to muscle cells.

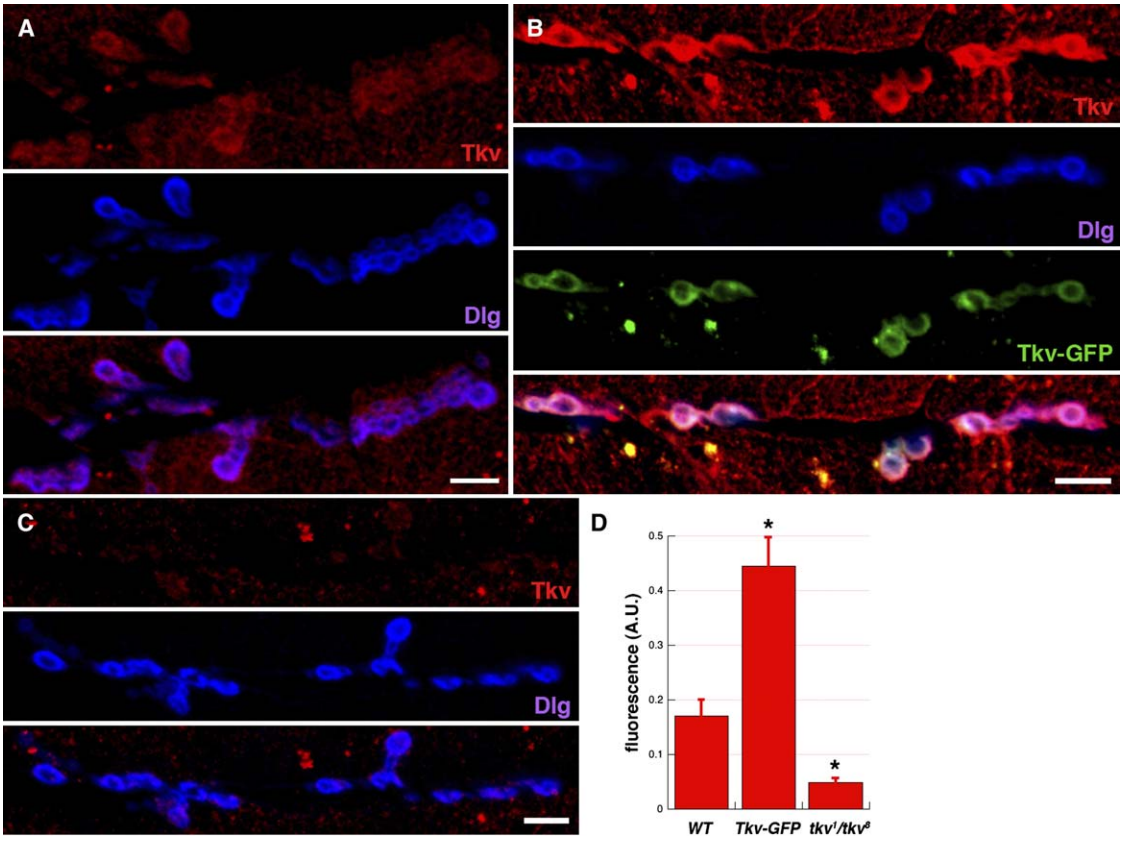

Figure S2. Specificity of the Tkv Immunostaining

(A–C) Staining of a muscle 6/7 NMJ showing Tkv (red) and Dlg (blue) immunostaining in wt (A), *MHC-GAL4/UAS-Tkv-GFP* (Tkv-GFP, green, [B]), and in a tkv^1/tkv^8 mutant (C). Scale bars equal 10 μm.

(D) Quantification of Tkv levels of average fluorescence (bars, standard errors) at the NMJ in wt (n = 10), *MHC-GAL4/UAS-Tkv-GFP* (n = 6), and tkv^1/tkv^8 mutants (n = 9). *p < 0.05.

where n^s_{mob} denotes the steady-state value of the mobile nuclear pool and $b = n_{tot}(0)/n^s_{tot}$ is the bleaching depth. Here, $n_{tot} = n_{mob} + n_{im}$ is the total nuclear concentration, n^s_{tot} is its steady-state value, and $n^s_{tot}(0)$ is its value after bleaching. The observed nuclear fluorescence per unit volume is proportional to n_{tot}. We therefore fit the measured fluorescence recovery *F(t)* (see equation 3) to the

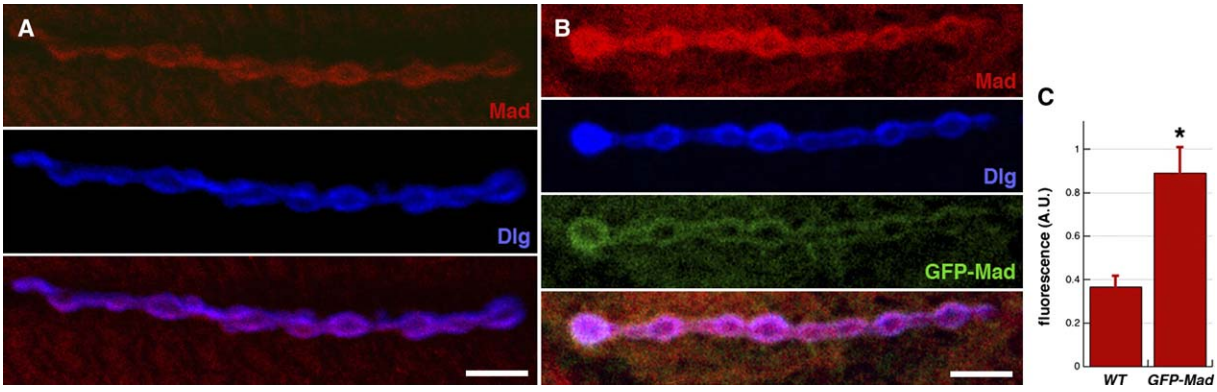

Figure S3. Specificity of the Mad Immunostaining

(A and B) Staining of a muscle 6/7 NMJ showing Mad (red) and Dlg (blue) immunostaining in wt (A) and *MHC-GAL4/UAS-GFP-Mad* (GFP-Mad, green, [B]). Scale bars equal 10 μm.

(C) Quantification of Mad levels of average fluorescence (bars, standard errors) at the NMJ in wt (n = 10) and *MHC-GAL4/UAS-GFP-Mad* (n = 14). *p < 0.05.

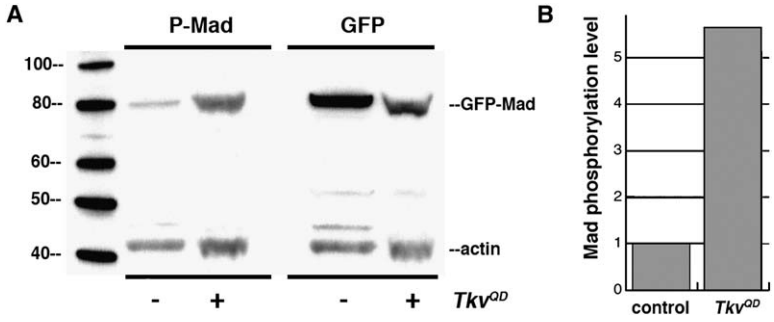

Figure S4. Mad Phosphorylation Levels

(A) Western blot of Phospho-Mad and Mad levels, detected by anti-P-Mad and anti-GFP antibodies in control ((−), *MHC-GAL4/UAS-GFP-Mad*) and Tkv^{QD} ((+), *MHC-GAL4::UAS-GFP-Mad/UAS-Tkv*^{QD}) muscles. In brief, 5–10 muscle fillets of each genotype were prepared as described in the Experimental Procedures section and the protein extract was used in a standard Western blot procedure. As a loading internal control, an anti-actin antibody (Sigma) was used. Image was acquired with a FUJI LAS 1000 imaging system.

(B) Quantification of Mad phosphorylation level. The signal for P-Mad and Mad were measured with Image Gauge and normalized according to the actin signal from the corresponding lane. The ratio P-Mad:Mad was calculated for control and Tkv^{QD} and is shown after normalization to the control level.

time dependence of the normalized nuclear concentration $F(t) = \left(n_{tot}(t) - n_{tot}(0)\right)/n^{s}_{tot}$. According to equation 7, *F(t)* is given by

$$F(t) = m(1-b)(1-e^{-K_e t}), \tag{8}$$

where $m = n^{s}_{mob}/n^{s}_{tot}$ is the nuclear mobile fraction. From equation 6 it follows that

$$K_i = mK_e n^{s}_{tot}/c^{s}, \tag{9}$$

where c^s is the cytosolic concentration in the steady state.

Kinetic Behavior of the Different Mad Species

In the previous description of the FRAP experiments, we considered three Mad pools. Now we discuss a situation where different phosphorylation states of Mad confer distinct import and export behaviors to the molecule. Therefore, we introduce a model based on five different Mad species to account for the concentrations of Mad and P-Mad molecules in the cytosol and in the nucleus. We assume that only the rate of Mad phosphorylation varies for the three different mutant conditions (control, Tkv^{QD}, and K^+), while all other rates such as nuclear import and export rates are the same for all these conditions. This assumption is consistent with experimental data, indicating that signaling is transduced by activation of the kinase activity of the receptor.

As shown in Figure 5B, we distinguish between two cytosolic and three nuclear Mad pools. Their kinetics are given by the following rate equations:

$$\begin{aligned}
\frac{dn_M}{dt} &= k_{in}c_M - k_{out}n_M \\
\frac{dc_M}{dt} &= \frac{V_n}{V_c}(k_{out}n_M - k_{in}c_M + k_d c_{PM} - k_p c_M) \\
\frac{dc_{PM}}{dt} &= \frac{V_n}{V_c}(k_p c_M - k_d c_{PM} + k'_{out}n_{PM} - k'_{in}c_{PM}) \\
\frac{dn_{PM}}{dt} &= k'_{in}c_{PM} - k'_{out}n_{PM} + k_{inact}n^{*}_{PM} - k_{act}n_{PM} \\
\frac{dn^{*}_{PM}}{dt} &= k_{act}n_{PM} - k_{inact}n^{*}_{PM}.
\end{aligned} \tag{10}$$

Here, n_M is the nuclear Mad concentration, n_{PM} is the nuclear P-Mad concentration, n^{*}_{PM} is the nuclear P-Mad* concentration, c_M is the cytosolic Mad concentration, c_{PM} is the cytosolic P-Mad concentration, k_{in} is the import rate of cytosolic Mad into the nucleus, k_{out} is the export rate of Mad from the nucleus, k'_{in} is the import rate of cytosolic P-Mad into the nucleus, k'_{out} is the export rate of P-Mad from the nucleus, k_p is the phosphorylation rate of cytosolic Mad, k_d is the dephosphorylation rate of cytosolic P-Mad, k_{act} is the activation rate of P-Mad in the nucleus, k_{inact} is the inactivation rate of P-Mad* in the nucleus, V_n is the volume of the nucleus, and V_c is the volume of the cytosol. The ratio V_n/V_c appears in equations 10 since an exchange of a molecule between cytosol and nucleus has a different effect on the cytosolic and nuclear concentration.

We assume that the FRAP experiments are initiated at a moment when the system has relaxed to the steady state(s). Therefore, the steady-state values of the concentrations are chosen as an initial condition for the theoretical description of the FRAP experiments. With equations 10, they can be expressed as

$$\begin{aligned}
n^{s}_{M} &= \frac{Y}{1+Z}\,c^{s}_{tot} \\
c^{s}_{M} &= \frac{1}{1+Z}\,c^{s}_{tot} \\
c^{s}_{PM} &= \frac{1}{1+1/Z}\,c^{s}_{tot} \\
n^{s}_{PM} &= \frac{Y'}{1+1/Z}\,c^{s}_{tot} \\
n^{*s}_{PM} &= \frac{XY'}{1+1/Z}\,c^{s}_{tot},
\end{aligned} \tag{11}$$

where $X = k_{act}/k_{inact}$, $Y = k_{in}/k_{out}$, $Y' = k'_{in}/k'_{out}$, and $Z = k_p/k_d$ are ratios of the exchange rates and c^{s}_{tot} is the steady-state total cytosolic concentration.

By bleaching the fluorescence in the nucleus, the concentration of fluorescent nuclear Mad is reduced to the fraction *b* (bleaching depth), while the cytosolic concentration of fluorescent molecules does not change. We assume here that the bleaching process occurs instantaneously.

In order to describe the recovery of the nuclear fluorescence after bleaching, we assume that the exchange of n^{*}_{PM} with n_{PM} via the rates k_{act} and k_{inact} is slow compared to the duration of the experiments (1000 s) and accounts for the immobile fraction. To describe the fluorescence recovery, we thus neglect the exchange by the rates k_{act} and k_{inact}. As the ratio V_c/V_n is of the order of 600, changes of the cytosolic concentrations during recovery can be ignored (see equation 10). With these assumptions, the FRAP kinetics are described by

$$\begin{aligned}
\frac{dn_M}{dt} &= k_{in}c_M - k_{out}n_M \\
\frac{dn_{PM}}{dt} &= k'_{in}c_{PM} - k'_{out}n_{PM} \\
\frac{dn^{*}_{PM}}{dt} &= 0.
\end{aligned} \tag{12}$$

The solution to these equations is

$$\begin{aligned}
n_M(t) &= n_{M,0}\left(1-(1-b)e^{-k_{out}t}\right) \\
n_{PM}(t) &= n_{PM,0}\left(1-(1-b)e^{-k'_{out}t}\right),
\end{aligned} \tag{13}$$

where the constants $n_{M,0}$ and $n_{PM,0}$ are equal to the steady-state values of the nuclear Mad and P-Mad concentrations n^{s}_{M} and n^{s}_{PM}, respectively, as given in equations 11. The recovery of the total nuclear concentration $n_{tot} = n_M + n_{PM} + n^{*}_{PM}$ determines the recovery of

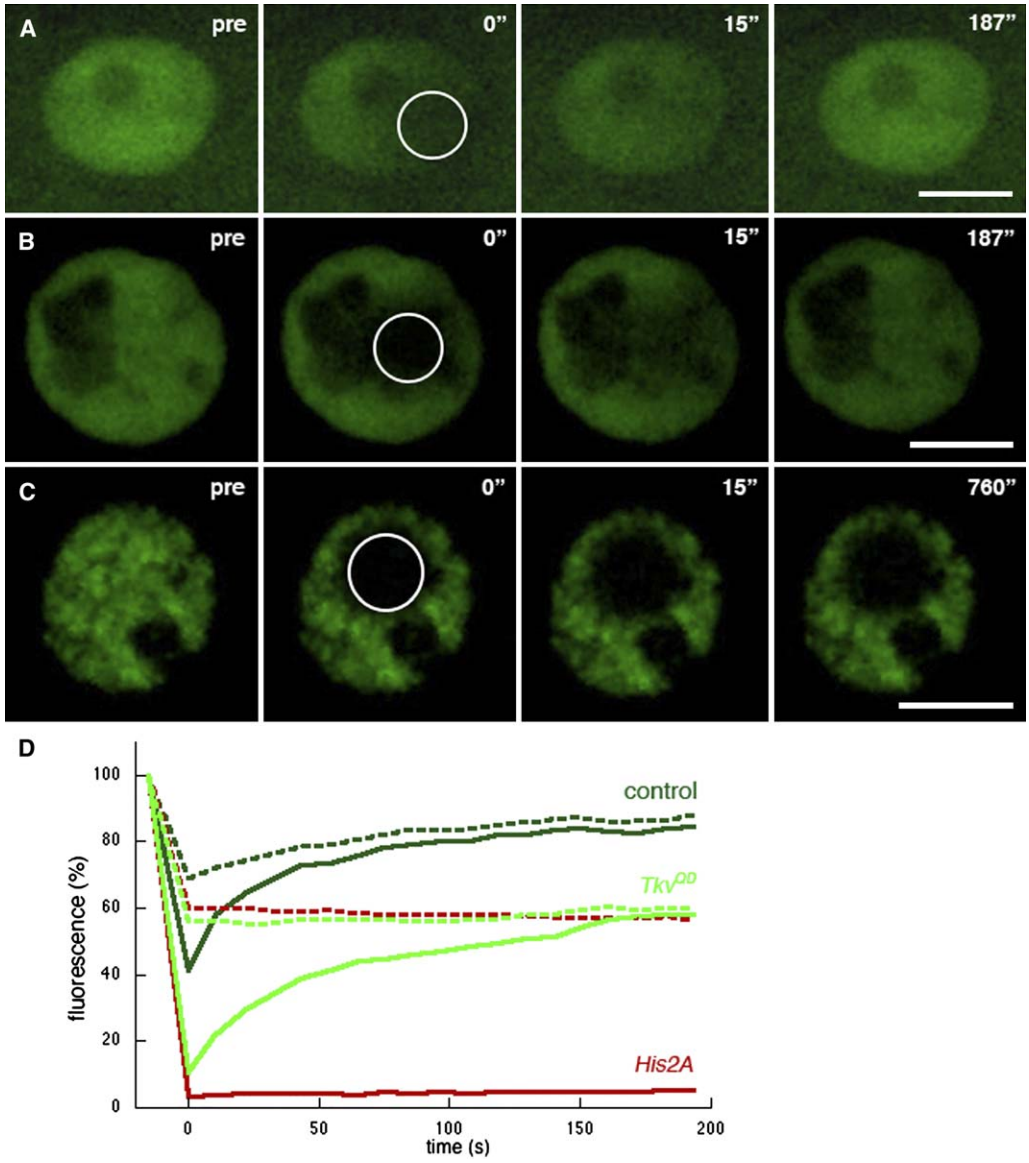

Figure S5. The “Immobile” Mad Is Not Anchored within the Nucleus

(A–C) FRAP experiments showing nuclei which were imaged before (pre) and after fluorescence photobleaching of GFP-Mad (A and B) or GFP-Histone2Av (C) in a small region within the nucleus (white circle) at the indicated times in control *MHC-GAL4/UAS-GFP-Mad* (A), *MHC-GAL4::UAS-GFP-Mad/UAS-Tkv^{QD}* (B), and *Ub-GAL4/UAS-His2Av-GFP* (C) animals. Scale bar equals 10 μm.

(D) Time course of the average fluorescence recovery in control (n = 9), *Tkv^{QD}* (n = 9), and *His2Av* animals (n = 2). Fluorescence is normalized to the prebleach value. Solid line, average fluorescence within the bleached region; dashed line, average fluorescence of the whole nucleus.

normalized fluorescence $F(t) = \left(n_{\mathrm{tot}}(t) - n_{\mathrm{tot}}(0)\right)/n^{\mathrm{s}}_{\mathrm{tot}}$ (see equation 3), which behaves thus as

$$F(t) = A(1-b)(1-e^{-k_{\mathrm{out}}t}) + B(1-b)(1-e^{-k'_{\mathrm{out}}t}), \qquad (14)$$

where $A = n^{\mathrm{s}}_{\mathrm{M}}/n^{\mathrm{s}}_{\mathrm{tot}}$ and $B = n^{\mathrm{s}}_{\mathrm{PM}}/n^{\mathrm{s}}_{\mathrm{tot}}$. We fit expression 14 to the experimental data by using the parameters A, B, k_{out}, and k'_{out} as fit parameters (see Figure 4F). This fit is done under the constraint that the fit parameters k_{out} and k'_{out} are the same for all three mutant conditions (control, *Tkv^{QD}*, and K^+). In principle, this leads to three different values $A_1 \ldots A_3$ and $B_1 \ldots B_3$ of the fit parameters A and B, which correspond to the three mutant conditions. Thus, if we include k_{out} and k'_{out}, there are in total eight fit parameters. Since we assume that the quantities X, Y, and Y' have the same values for all these mutant conditions and that only Z differs, additional constraints for the six values A_i and B_i are imposed. According to equations 11, they can be expressed as

$$X = \frac{1 - A_i - B_i}{B_i}$$
$$Y' = \frac{Y\,B_i}{Yc^{\mathrm{s}}_{\mathrm{tot,i}}/n^{\mathrm{s}}_{\mathrm{tot,i}} - A_i}, \qquad (15)$$

where i = 1, 2, or 3 corresponds to the three mutant conditions and the ratio $c^{\mathrm{s}}_{\mathrm{tot}}/n^{\mathrm{s}}_{\mathrm{tot}}$ is measured independently in the steady state (see Figure 4C, except for the K^+ condition for which the measured value is unreliable as discussed below). Considering these constraints, we effectively reduce the number of free fit parameters by replacing the six parameters A_i and B_i by the parameters X, Y, and Y'. From the fit of the experimental data, we can obtain the values for k_{out} and k'_{out},

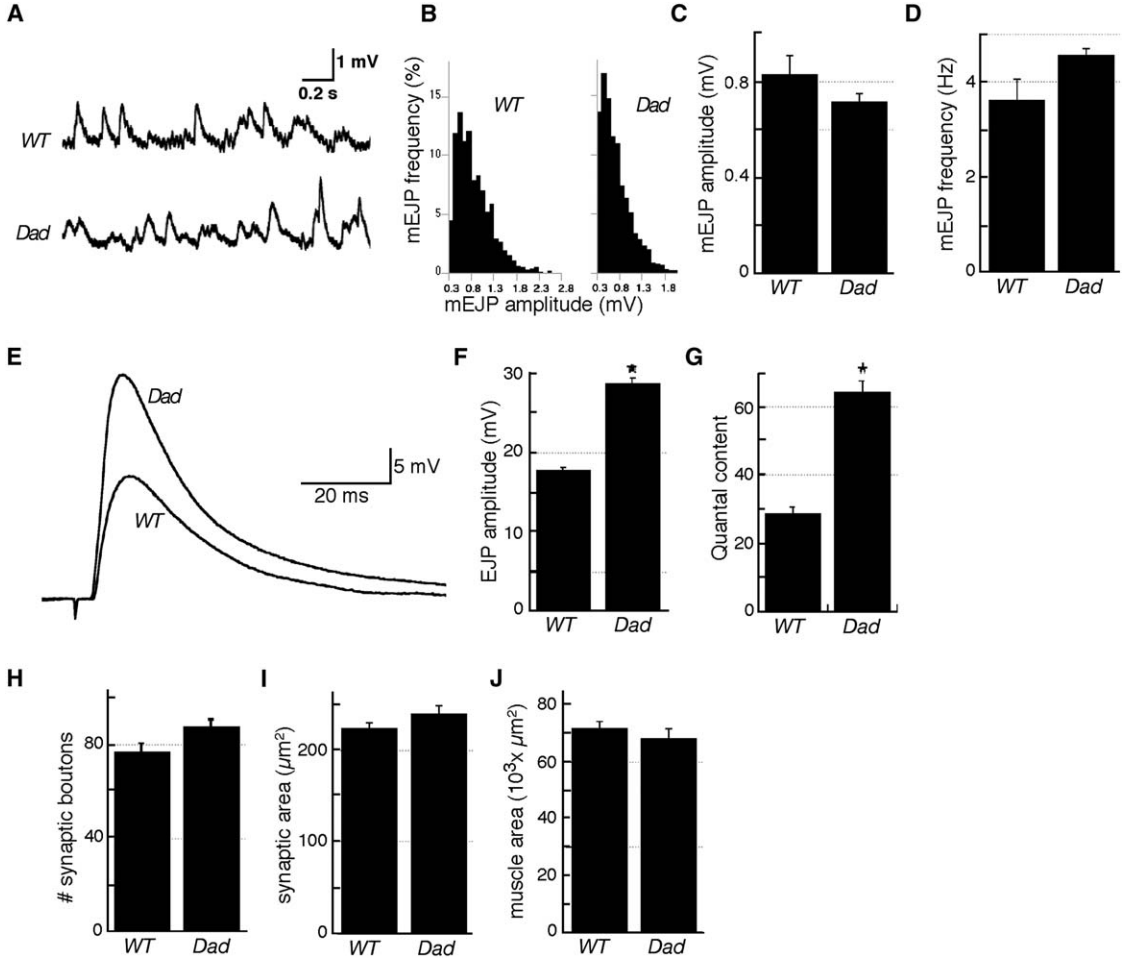

Figure S6. Neurotransmitter Release Is Affected when TGF-β Signaling Is Impaired

(A) Spontaneous mEJP traces from wild-type (wt) and *MHC-GAL4/UAS-Dad* (*Dad*)-expressing muscle 6.

(B) mEJP amplitude frequency distribution from wt (n = 1089 events) and *Dad*-expressing muscle 6 (n = 1909 events).

(C) Mean mEJP amplitude (mV; wt = 0.83 ± 0.16, n = 5; *Dad* = 0.72 ± 0.08, n = 7). No statistically significant difference can be observed. Bars correspond to standard errors.

(D) Mean mEJP frequency (Hz; wt = 3.63 ± 0.44, n = 5; *Dad* = 4.54 ± 0.14, n = 7). No statistically significant difference can be observed. Bars correspond to standard errors.

(E) Representative nerve-evoked EJP traces from wt and *Dad*-expressing muscle 6.

(F) Mean EJP amplitudes in wt and *Dad*-expressing muscle 6 (wt = 18.03 ± 0.46 mV, n = 5; *Dad* = 28.66 ± 2.04 mV, n = 7). *p < 0.05. Bars correspond to standard errors.

(G) Mean quantal content (wt = 28.7 ± 1.72, n = 5; *Dad* = 64.88 ± 3.12, n = 7). *p < 0.05. Bars correspond to standard errors.

(H–J) Synaptic bouton number (H), synaptic area (I), and muscle area (J) in wild-type and *Dad*-expressing muscle 6/7. No difference can be observed. Bars correspond to standard errors.

Procedures: Current clamp recordings in HL3 containing 0.75 mM Ca^{2+} were performed as previously described [S2] with some modifications. The mean EJP amplitude was determined by averaging single EJPs evoked at 1 Hz from at least five preparations, analyzed with Axograph Software (Axon Instruments, Inc.). The quantal content was calculated by dividing the mean EJP amplitude of a certain muscle by the mean mEJP recorded in the same muscle and was corrected for nonlinear summation. mEJPs were recorded for 1 min after the EJPs at 1 Hz and were analyzed with the event detection of Axograph Software.

For quantification of the synaptic area of NMJs from muscles 6/7, an anti-CSP staining was performed for at least nine preparations. Z-section images spanning the whole NMJ were acquired. The synaptic area was determined by projecting the aquired z-section images and thresholding them with MetaView software (Visitron Systems).

X, Y, and Y'. By using the constraints given in equation 15, we can determine all six corresponding values A_i and B_i. The values of the quantity $Z = k_p/k_d$ for the three mutant conditions are determined according to the equations 11:

$$Z_i = \frac{Y\, c^s_{tot,i}}{A_i\, n^s_{tot,i}} - 1. \qquad (16)$$

Here, the three different values of Z_i correspond to changes in the phosphorylation rate k_p for the three different conditions. The values of all parameters obtained by this fit are given in Table 1.

We can relate this model to the simple phenomenological description based on only three Mad pools, as introduced above. These pools can be related to the five pools discussed here: $c = c_M + c_{PM}$, $n_{mob} = n_M + n_{PM}$, and $n_{im} = n^*_{PM}$. Moreover, the effective import and export rates can be related to the specific rates:

$$K_i = \frac{k_{in} c^s_M + k'_{in} c^s_{PM}}{c^s_M + c^s_{PM}}$$
$$K_e = \frac{k_{out} n^s_M + k'_{out} n^s_{PM}}{n^s_M + n^s_{PM}}. \qquad (17)$$

The calculated values of these quantities, according to the fit results given in Table 1, are consistent with the values found by the single exponential fits (see Figure 4G). The two fit functions, 8 and 14, derived in the phenomenological description and the specific model, respectively, describe the experimental data well (see Figures 4E and 4F). As the mobile nuclear pool for the control and K^+ conditions consists mainly of nonphosphorylated Mad (see Table 1), expression 14 is dominated by the term $A(1-b)(1-e^{-k_{out}t})$. Conversely, in the case of Tkv^{QD}, the mobile nuclear pool mainly contains phosphorylated Mad (see Table 1) so that equation (14) is dominated by the term $B(1-b)(1-e^{-k'_{out}t})$. Thus, the single exponential fit 8 represents a good approximation of the double exponential fit 14 for the three mutant conditions. Note, however, that the double exponential fit allows us to determine the changes of the phosphorylation rate k_p in the different conditions and can account for the different mobile fractions.

The Case of the K^+ Stimulation Experiment

The effective import rates in the phenomenological description and some of the parameters (specific import rates, ratios of exchange rates, and pool sizes) in the specific model are calculated with the ratios c^s_{tot}/n^s_{tot} (concentration of the total cytosolic over the total nuclear Mad in the steady state; see equations 9, 15, and 16). In the case of the control and Tkv^{QD} experiments, these concentrations can be determined experimentally and correspond to the average fluorescence in the cytosol and nucleus before the FRAP experiment. However, this is not true for the K^+ stimulation experiment. In this case, before stimulation, the system is in the steady state corresponding to the control. The bleaching of fluorescence occurs 2 min after initiation of the K^+ stimulation, and therefore the system did not have enough time to relax from the control steady state to a new steady state caused by the stimulation. In principle, this relaxation would take hours. Thus, our experimental estimates of the steady-state values of the total nuclear and cytosolic Mad concentrations under this condition are unreliable.

Therefore, we have used the value of c^s_{tot}/n^s_{tot} in the K^+ condition as an additional fit parameter that reflects the fact that its measured value might be incorrect. With this procedure, we find $c^s_{tot}/n^s_{tot} \approx 0.22$ in the K^+ condition, while the measured value is about 0.31. This difference confirms that for this condition the measured value is unreliable. Indeed, this measured value does not lead to a reasonable fit of the fluorescence recovery to the experimental data. In summary, the values for the rates obtained in the K^+ condition should serve only as an indication that the signaling state during stimulation is different that in its absence, rather than as a quantitative assessment of the levels of signaling.

Supplemental References

S1. Kimura, H. (2005). Histone dynamics in living cells revealed by photobleaching. DNA Repair (Amst.) *4*, 939–950.

S2. Wucherpfennig, T., Wilsch-Bräuninger, M., and González-Gaitán, M. (2003). Role of *Drosophila* Rab5 during endosomal trafficking at the synapse and evoked neurotransmitter release. J. Cell Biol. *161*, 609–624.